

Solvothermal synthesis of ZnO nanoparticles at low temperatures as cathode buffer layers for polymer solar cells with an inverted device structure

Jie Luo¹ · Qian Liu¹ · Yong Zhang² · Wei Zhang¹ · Zuyong Feng¹ · Peiju Hu¹

Received: 4 March 2016 / Accepted: 8 June 2016 / Published online: 14 June 2016
© Springer Science+Business Media New York 2016

Abstract Inverted polymer solar cells of the conventional poly(3-hexylthiophene) (P3HT):(6,6)-phenyl-C61butyric acid methyl ester (PC₆₁BM) blend on indium tin oxide substrates were fabricated. By using mixed-solvent dispersed ZnO nanoparticles (NPs) as cathode buffer layer, device performances are improved obviously. ZnO NPs with a size of 3–5 nm synthesized by solvothermal synthesis at 65 °C show relatively wide photoluminescence peak of 300–650 nm. Based on Hansen solubility parameter theory, a mathematical method was applied to calculate the Hansen solubility parameters of bi-solvent system to disperse ZnO NPs and the proportion of each component in the mixed solvent. This excellent dispersion for ZnO NPs in the bi-solvent system has a important influence on the performance of the device. Compared to other methods of ZnO nanofilm fabrication, this method reveals a simple, convenient, moderate and effective way to manufacture the favorable buffer layer in organic solar cells.

1 Introduction

Polymer organic solar cells (OSCs) are expected to be alternative energy resource for future generation and likely to be commercializing very soon [1–3]. The highest power conversion efficiency (PCE) of a single junction organic

solar cell can be over 8 % [4], and a tandem polymer solar cell can reach the PCE higher than 10 % [5] nowadays.

Conventional organic solar cells usually contain an anode buffer layer, typically poly(3,4-ethylenedioxythiophene)–poly-(styrenesulfonate) (PEDOT:PSS) on indium tin oxide (ITO) glass as the anode, and a low work-function metal, typically Al, and a photoactive organic blend layer as an active layer was sandwiched between the anode and the cathode. However, PEDOT:PSS is unstable because it is easy to adsorb water and form the insulating domains, and the interface between ITO and PEDOT:PSS is not stable because PEDOT:PSS is acidic and can etch ITO, thus degrading the performance of devices [6–8].

One approach to resolve the problems is to adopt the inverted geometry. In the inverted structure the interface of ITO/PEDOT:PSS can be avoided by using various high band gap n-type of oxides [9–12], such as ZnO, TiO₂ and SnOx. Among these materials, ZnO is more attractive for its high optical transparency, environmentally friendly nature, relatively higher electron mobility, Ohmic contact with the organic layer and blocking capability for the UV-light induced photodegradation of organic materials. To add a thin layer of ZnO into inverted organic solar cells, different methods, including the magnetron sputter, MOCVD, CVD, ALD, sol-gel, solvothermal and ZnO (NPs) methods, can be utilized [13, 14]. From the consideration of the economy, process and environmental protection, the solvothermal is the best in these methods. Moreover, due to simple and effective, the method is the most widely used solution method in the synthesis of nanomaterials. ZnO NPs were simply synthesized from zinc acetate dihydrate with addition of strong bases dissolved in methanol and spin-coated onto bottom electrodes to form buffer layers at low temperature [15, 16]. However, ZnO NPs synthesized in solvothermal method faced large

✉ Jie Luo
jlueo@gdut.edu.cn

¹ School of Physics and Optoelectronic Engineering, Guangdong University of Technology, Guangzhou 510006, China

² Institute of Optoelectronic Materials and Technology, South China Normal University, Guangzhou 510631, China

scale coacervated morphology in organic solar cells, which limited the PCE and stabilities. In particular, the surface roughness of ZnO buffer layer can affect the photovoltaic performance of organic solar cells by changing the effective interfacial area between the active layer and the ZnO buffer layer. In order to prepare ZnO buffer layers for highly efficient organic solar cells, homogeneous colloidal solution of ZnO NPs without aggregation are pivotal [17].

To prepare solution for further deposition process in organic solar cells, ZnO NPs were dispersed in non-polar solvents such as chloroform, chlorobenzene, etc. [16, 18, 19]. Normally, the method of addition surfactant and polar solvent is used in uniform dispersion of ZnO NPs. However, significant loss of electron transport is expected through insulating surfactant interface [20].

In this study, a solution method, the solvothermal, is used to synthesize the ZnO NPs at a very low temperature of 65 °C in polytetrafluoroethylene autoclave (TFT). The size of ZnO NPs synthesized is about 3–5 nm. Moreover, we demonstrate that three kinds of mixed solvent, non-polar and polar, which can remarkably improve dispersion of ZnO NPs by modifying hydrogen bonding interaction of solvents. The mixed solvent using methanol and chloroform is the most widely used to disperse ZnO NPs in the inverted solar cell [21, 22]. In this study, *o*-dichlorobenzene was used as a dispersant displays better performance relative to chloroform. It was shown that both morphology of ZnO buffer layers and the PCE of the organic solar cells having blend of poly(3-hexylthiophene) (P3HT) and (6,6)-phenyl-C61-butyric acid methyl ester (PC₆₁BM) as the active layer were improved using nearly transparent colloidal solution of ZnO NPs.

2 Experimental

2.1 Synthesis

For the solvothermal method, 0.018 mol of zinc acetate dihydrate (ZnOAc) was dissolved in 50 ml of methanol and 0.04 mol of NaOH solid was dissolved in 20 ml of methanol. Once all of the ZnOAc and NaOH was fully dissolved, the all of NaOH solution was dropped to ZnOAc solution using syringe pump with rate of 2 ml min⁻¹. The solution mixture was further reacted in polytetrafluoroethylene autoclave for 12 h at 65 °C. A white ZnO NPs was obtained, which was then extracted by precipitation with centrifugation at room temperature. The precipitate was further cleaned by centrifugation and washed three times with methanol to remove excess alkali. Then, the precipitates were dried in dryer at room temperature to remove residual methanol. Finally, the ZnO NPs were dispersed in solvent based on methanol chlorobenzene and

isopropyl alcohol having various volumetric ratio of each component, including chlorobenzene, isopropyl alcohol and trichloromethane.

2.2 Solar cell fabrication

The layer structure of the device in this work featured a inverted structure, ITO/ZnO NPs/P3HT:PCBM/MoO₃/Ag. The solution of P3HT:PCBM (1:0.8 by weight, 20 mg ml⁻¹) in 1,2-dichlorobenzene was prepared by stirring for 12 h at 50 °C. Indium–tin oxide (ITO: the thickness is 120 nm, the sheet resistance ≤15 Ω/square) substrates were cleaned by ultrasonication with acetone, distilled water, detergent, distilled water, acetone and isopropanol each for 10 min and was subsequently dried in oven at 90 °C. The substrates and the reagent were then moved into a nitrogen-filled glove-box. The next procedure is carried out in the nitrogen-filled glove-box. The ZnO NPs dispersed in mixture solvents with the concentration of 20 mg/ml were spin-coated onto cleaned ITO substrates, and the film thickness was around 30 nm, followed by annealed in the heating stage at 80 °C for 20 min. The solution of poly-3-hexylthiophene (P3HT) and (6,6)-phenyl-C61-butyric acid methyl ester (PCBM) in 1,2-chlorobenzene with the concentration of 20 mg/ml and 1:0.8 weight ratio was spin coated on the top of ZnO films at 800 rpm for 45 s to form the active layer. The devices were then annealed at 150 °C for 10 min. Finally, the MoO₃/Ag anode was thermally evaporated onto the top of the active layer through a shadow mask in a vacuum of about 2 × 10⁻⁴ Torr. The thicknesses of MoO₃ and Ag were 7 and 120 nm separately.

2.3 Characterization

The shape and the crystal structure of ZnO NPs were characterized by transmission electron microscopy (TEM) on a JEM-2100 and X-ray diffraction (XRD) with XD-2 (CuKα, 36 kV, 20 mA), respectively. Electronic absorption spectra were checked by a HP 8453 UV–Vis spectrophotometer. Surface topography and roughness of the ZnO NPs were measured using atomic force microscopy (AFM). AFM measurements were operated in tapping mode using a Veeco dimension V atomic microscope. Film thickness measurement was carried on profile meter (Dektak150). The current–voltage (J–V) characterization was measured at an illumination intensity of 100 mW/cm² with an AM1.5 solar simulator. The current density–voltage (J–V) characteristics of the OSC devices in the dark and under illumination were measured with a Keithley 236 source-measure unit. The power conversion efficiency (PCE) and fill factor (FF) were calculated according to the following equations [23–25]:

$$PCE = FF \times J_{sc} \times V_{oc} / P_{in}$$

$$FF = I_m V_m / J_{sc} V_{oc}$$

where P_{in} is the incident radiation flux, J_{sc} and V_{oc} are the short circuit current and open circuit voltage, respectively. I_m and V_m are the current and voltage at the maximum power output, respectively.

3 Results and discussion

3.1 Characterization of ZnO NPs and film

XRD patterns of as-prepared sample is shown in Fig. 1a, in which the reflection peak can be assigned to the pure crystalline of ZnO NPs, and it exhibits hexagonal wurtzite structure. The broad peaks displayed in the spectra indicate the small size of the ZnO NPs and the more defect of crystal. TEM images of the ZnO NPs synthesized by using solvothermal method at 65 °C were shown in Fig. 1b. The nanocrystals were spherical, which size from 3 to 5 nm. This indicates that the solvothermal method can be used to provided monodispersed nanorods, which is helpful to fabricate solar cell.

Figure 2a presents UV–Vis absorption spectrum of ZnO NPs dispersed in mixed solvent. The excitonic shoulder peak at around 360 nm is related to the near band edge emission of ZnO. This indicated that the ZnO thin film only blocks the light with a wavelength shorter than 370 nm, which allows maximum amount of light to pass through the active organic layer. Figure 2b shows the PL spectrum of the ZnO films spinning on quartz glass. The intrinsic peak at the 330–370 nm range is related to the near band edge emission of ZnO, this also reflects on UV–Vis absorption spectrum of ZnO NPs. The wide peaks at the 370–650 nm range are due to the defects, including Zn_i (interstitial Zn atom), O_i , V_O (oxygen atom vacancy), V_{Zn} , V_O^+ , V_O^{2+} , and

so on [26–28]. Figure 2c shows UV–Vis transmittance spectrum of ZnO NPs dispersed in mixed solvent and spinning on quartz glass. The transmittance is about 95 % at the 370–1000 nm. As is known, the ZnO NP films is used as an excellent optically transparent interlayer in the visible light range as cathode buffer layer. However, The transmittance drops rapidly at the 200–370 nm (<5 %). It shows the excellent quality of ZnO NPs dispersed in mixed solvent.

3.2 Characterization and analysis of device

Hansen solubility parameters (HSP) theory have offered useful methods to understand and investigate dispersion or solubility of pigments and polymers [29]. It can also be used to explore dispersion of metallic oxide, such as ZnO NPs. The total solubility parameter (δ_t), the dispersion component parameter (δ_d), the polar component parameter (δ_p) and the hydrogen bonding component parameter (δ_h) were calculated according to the following equations:

$$\delta_t = [(\Delta H - RT) / V_m]^{1/2}$$

$$\delta_t = (\delta_d^2 + \delta_p^2 + \delta_h^2)^{1/2}$$

where δ_t is defined as the square root of the cohesive energy density which is the energy required to infinitely separate a unit volume of a given species from the other component, ΔH is heat of vaporization, R is gas constant, T is temperature and V_m is the unit of molecular weight, respectively.

The HSPs of ZnO NPs were determined by solvent screening through associating the solubility parameters of the solute with the most successful solvents using HSPiP, a software developed by S. Abbott and H. Yamamoto based on HSP theory [30, 31]. The HSPs of ZnO NPs were calculated to be $\delta_d = 17.25 \text{ MPa}^{1/2}$, $\delta_p = 6.75 \text{ MPa}^{1/2}$ and $\delta_h = 10.83 \text{ MPa}^{1/2}$ with the interaction radius of

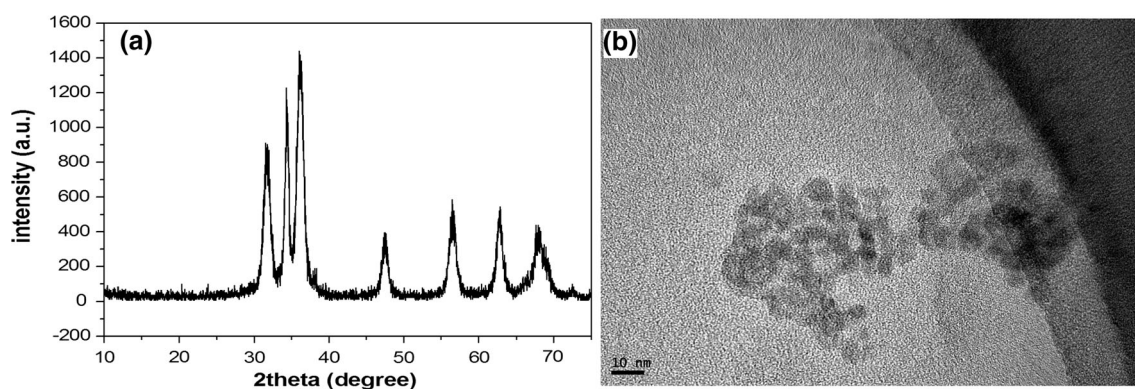


Fig. 1 XRD spectra of ZnO nanoparticle powder (a) and TEM of ZnO NPs (b)

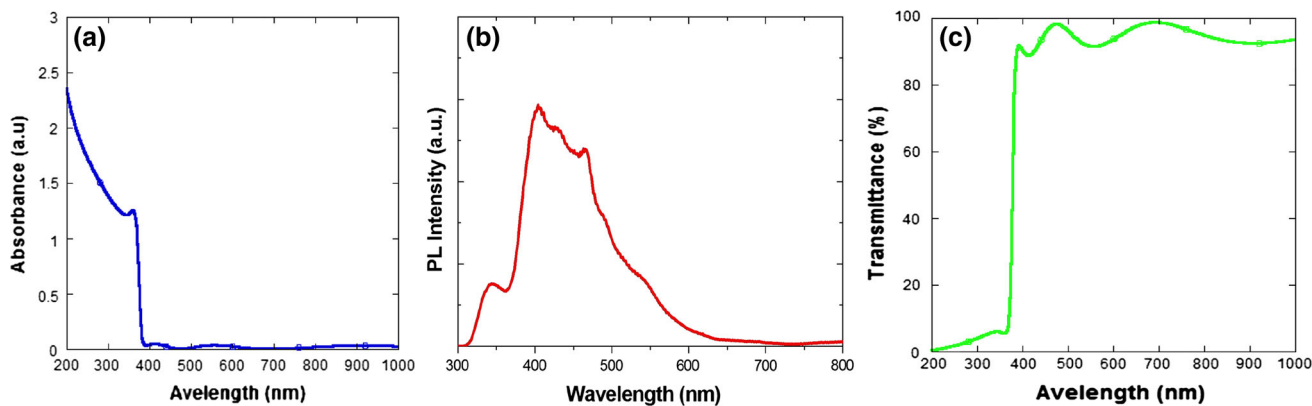


Fig. 2 UV-Vis absorption spectra of ZnO films on quartz glass (a), PL spectrum of ZnO films on quartz glass (b) and UV-Vis transmittance spectra of ZnO films on quartz glass (c)

$R_o = 6.7 \text{ MPa}^{1/2}$. Here, the R_o is the interaction radius of the dispersion of ZnO NPs in solvents which designates the radius of the sphere in HSP space indicating maximum tolerance of the solution. Table 1 reveals solubility parameter (HSPs) and boiling point of solvents and ZnO NPs which is used in this study. For a specific solvent distance between ZnO NPs (R_a) is defined as equations:

$$R_a^2 = 4(\delta_{d1} - \delta_{d0})^2 + (\delta_{p1} - \delta_{p0})^2 + (\delta_{h1} - \delta_{h0})^2$$

where subscripts 1 and 0 represent the solvent and the solute (ZnO NPs). Then, for a solvent, the solute will be dispersed when $R_a < R_o$ which means that the HSPs of solvent is within the R_o of the solute.

In this study, the ZnO cathode buffer layer is deposited from the solution of ZnO NPs dispersed in mixed solvent (non-polar and polar solvent) [32]. The non-polar solvent we used is dichlorobenzene and chloroform, and the polar solvent is methanol and isopropanol. For mixtures of two solvents, due to the solubility parameters of mixtures are linear [29], the HSPs can be calculated according to the following equations:

$$\delta_i = x\delta_{i1} + (1 - x)\delta_{i2} \quad (i = d, p, h; \quad 0 < x < 1)$$

Here, subscripts 1 and 2 represent two different solvents; “ x ” is the volumetric fraction of one of solvents. So, for two different solvents distance between ZnO NPs (R_a) is defined as equations:

$$R_a^2 = 4[x\delta_{d1} + (1 - x)\delta_{d2} - \delta_{d0}]^2 + [x\delta_{p1} + (1 - x)\delta_{p2} - \delta_{p0}]^2 + [x\delta_{h1} + (1 - x)\delta_{h2} - \delta_{h0}]^2$$

Through the inequality of $R_a < R_o$ and the equality of $R_o = 6.7 \text{ MPa}^{1/2}$ (ZnO NPs), the following quadratic inequations can be obtained:

$$ax^2 + bx + c < 0$$

Here, coefficient of “ a ”, “ b ” and “ c ” are calculated as equations:

$$a = 4(\delta_{d1} - \delta_{d2})^2 + (\delta_{p1} - \delta_{p2})^2 + (\delta_{h1} - \delta_{h2})^2$$

$$b = 8(\delta_{d1} - \delta_{d2})(\delta_{d2} - \delta_{d0}) + 2(\delta_{p1} - \delta_{p2})(\delta_{p2} - \delta_{p0}) + 2(\delta_{h1} - \delta_{h2})(\delta_{h2} - \delta_{h0})$$

$$c = 4(\delta_{d2} - \delta_{d0})^2 + (\delta_{p2} - \delta_{p0})^2 + (\delta_{h2} - \delta_{h0})^2 - R_o^2$$

$$\Delta = b^2 - 4ac$$

Under the condition of $0 < x < 1$ and $\Delta > 0$, the solution of quadratic inequation is the dissolved components we need. Combined with a minimal solution of quadratic equations, the most appropriate dissolved components can be calculated according to the following equations:

$$x_{\min} = -b/2a$$

In the end, the HSPs and “ x ” of mixtures are obtained according to the preceding method and HSPs of Table 1

Table 1 The solubility parameter (HSPs) and boiling point of solvents and ZnO NPs

	δ_d (MPa ^{1/2})	δ_p (MPa ^{1/2})	δ_h (MPa ^{1/2})	δ_t (MPa ^{1/2})	R_a	Boiling point (°C)
Chloroform	17.8	3.1	5.7	19	6.39	61.5
<i>o</i> -Dichlorobenzene	19.2	6.3	3.3	20.5	8.49	180.4
Methanol	15.1	12.3	22.3	29.6	13.45	64.7
Isopropanol	15.8	6.1	16.4	23.5	6.31	82.45
ZnO NPs	17.25	6.75	10.83	21.46		

Table 2 The solubility parameter (HSPs) and the volumetric fraction of mixtures

Solvent	δ_d (MPa ^{1/2})	δ_p (MPa ^{1/2})	δ_h (MPa ^{1/2})	δ_t (MPa ^{1/2})	x	Ra
A	16.98	5.91	10.76	20.95	0.695	1
B	16.79	4.61	11.09	20.64	0.496	1.49
C	17.63	8.60	10.58	22.29	0.617	1.95
D	17.25	6.19	10.84	21.29	0.426	0.56

The “A” “B” “C” “D” are the mixtures of chloroform–methanol, chloroform–isopropanol, *o*-dichlorobenzene–methanol and *o*-dichlorobenzene–isopropanol, respectively

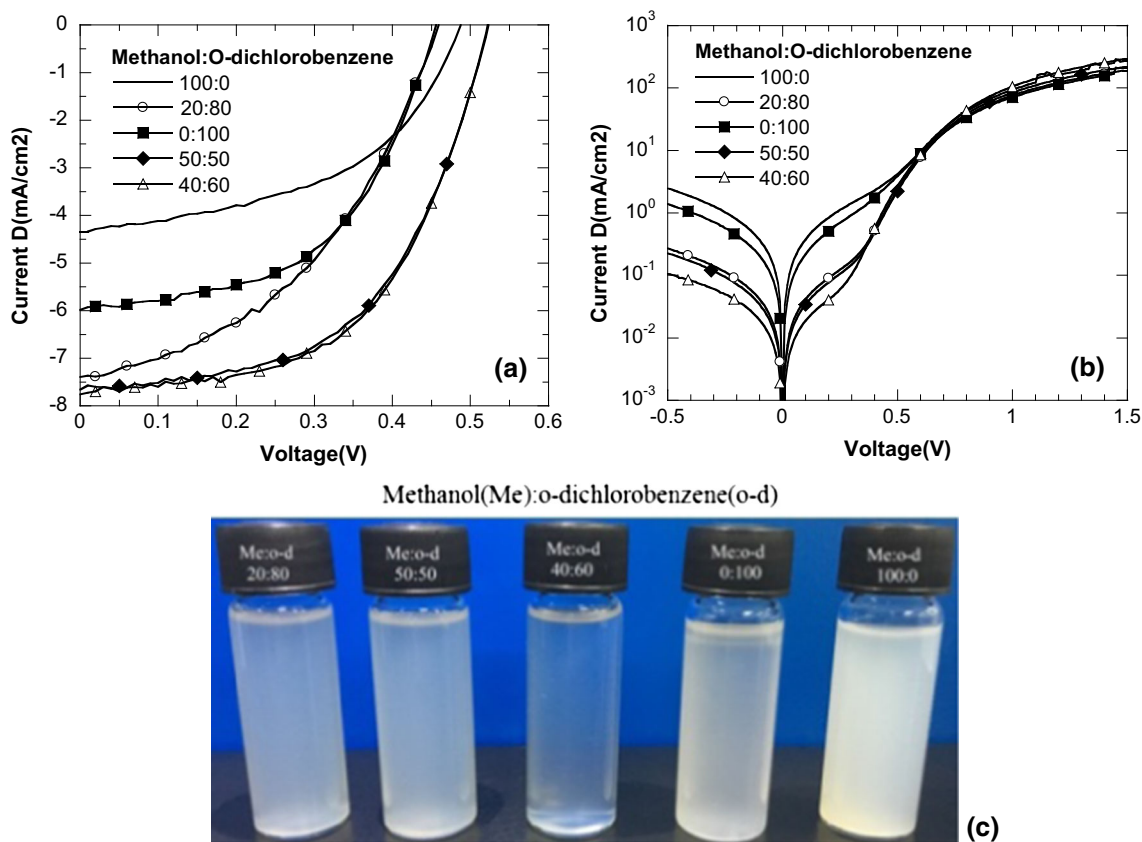


Fig. 3 Illuminated (a) and dark (b) J–V characteristics of the inverted organic solar cells with buffer layers deposited from the ZnO NPs solution with different ratios mixture of methanol/*o*-dichlorobenzene solvents. The number “100:0” “20:80” “40:60” “50:50” “0:100” are the mixtures of 100 % *o*-dichlorobenzene,

20 % methanol + 80 % *o*-dichlorobenzene, 40 % methanol + 60 % *o*-dichlorobenzene, 50 % methanol + 50 % *o*-dichlorobenzene, 100 % methanol. **c** the photographs of ZnO NPs solutions with different methanol/*o*-dichlorobenzene ratios

reveals. As shown in Table 1, The Ra of pure solvent are approximated to Ro (Ro = 6.7) or outnumber Ro, it shows that the pure solvent is difficult to disperse ZnO NPs. Solubility parameter (HSPs) and the volumetric fraction of mixtures calculated by the preceding method are revealed in Table 2. As shown in this table, the best mixtures are “D” (*o*-dichlorobenzene-isopropanol) which HSPs is in good agreement with HSPs of ZnO NPs. The Ra of mixtures of chloroform–methanol, chloroform-isopropanol and *o*-dichlorobenzene–methanol are far less than Ro, it means the three mixtures are also “good” solvents showed highly improved dispersion of ZnO NPs.

Table 3 The photovoltaic properties of the inverted organic solar cells with buffer layers deposited from the ZnO NPs solution dispersed in different mixture of methanol/*o*-dichlorobenzene (DCB) solvents

Methanol:DCB	J_{sc} (mA/cm ²)	V_{oc} (V)	FF (%)	PCE (%)
100:0	7.39	0.46	0.44	1.48
20:80	6.37	0.50	0.54	1.71
40:60	7.76	0.52	0.55	2.22
50:50	7.66	0.52	0.55	2.19
0:100	7.19	0.43	0.35	1.07

Current density–voltage (J–V) characteristics of OSC with ZnO buffer layer under AM 1.5G irradiation with intensity of 100 mW/cm² and in dark are shown in Fig. 3. ZnO films are deposited from mixture solvents of methanol/*o*-dichlorobenzene with different composition. The photographs of ZnO NPs solutions with different methanol/*o*-dichlorobenzene ratios are shown in Fig. 3c. It can be seen that when the volume ratio reaches 40:60 %, ZnO NPs are easily dispersed in the mixture solvents of methanol/*o*-dichlorobenzene without any sign of aggregation. Table 3 summarizes the data of device parameters. It can be observed that the device based on ZnO NPs dispersed in pure methanol exhibits the lowest PCE of 1.07 %. With the volume ratio of methanol/*o*-dichlorobenzene changing from 100:0 to 40:60 %, the V_{oc}, J_{sc}, and FF of devices increase gradually, the PCE increases from 1.07 to 2.22 %. When the volume ratio reaches 40:60 %, the device achieves V_{oc} of 0.52 V, J_{sc} of 7.76 mA/cm², and FF of 0.55, giving the highest PCE of 2.22 %. However, when the volume ratios are under 40:60 % and eventually change into pure *o*-dichlorobenzene, OSCs show obvious degradations in the J_{sc}, V_{oc}, FF and PCE. Moreover, the optimized volume ratio of binary solvents is 40:60 %, which is conform to the volumetric fraction of *o*-dichlorobenzene-methanol calculated by the preceding mathematical

method. It indicates that this calculation method is correct and very meaningful for other devices.

To reveal the effect of aggregation variation on the surface morphology of ZnO nanofilm, the AFM are employed to investigate the surface morphology of ZnO nanofilm [33]. As shown in Fig. 4, the root-mean-square (RMS) roughness value of ZnO films made from the pure methanol condition is 22.8 nm. The increased pore size and the aggregation of ZnO NPs can be apparently found in the film, indicating that the film is an uncontinuous film with large roughness. When the *o*-dichlorobenzene is added and the mixed (methanol/*o*-dichlorobenzene) volume ratios are changed into 100:0 to 40:60 %, the RMS roughness and the void size of ZnO films decrease dramatically and the dense films were formed. With the solvents ratios changed to 40:60 %, the ZnO films is smoothest with a lowest RMS roughness of 4.4 nm. And, the dense and homogeneous of ZnO films is obtained. However, further change of solvent ratios to 50:50 and 20:80 % results in increased roughness and void size. And, the dense and homogeneous of ZnO films is very poor. The RMS variations from AFM measurements are conform to the volumetric fraction of *o*-dichlorobenzene-methanol calculated by the preceding method and the efficiency of the device. More importantly, it also indicates that our calculation method is correct.

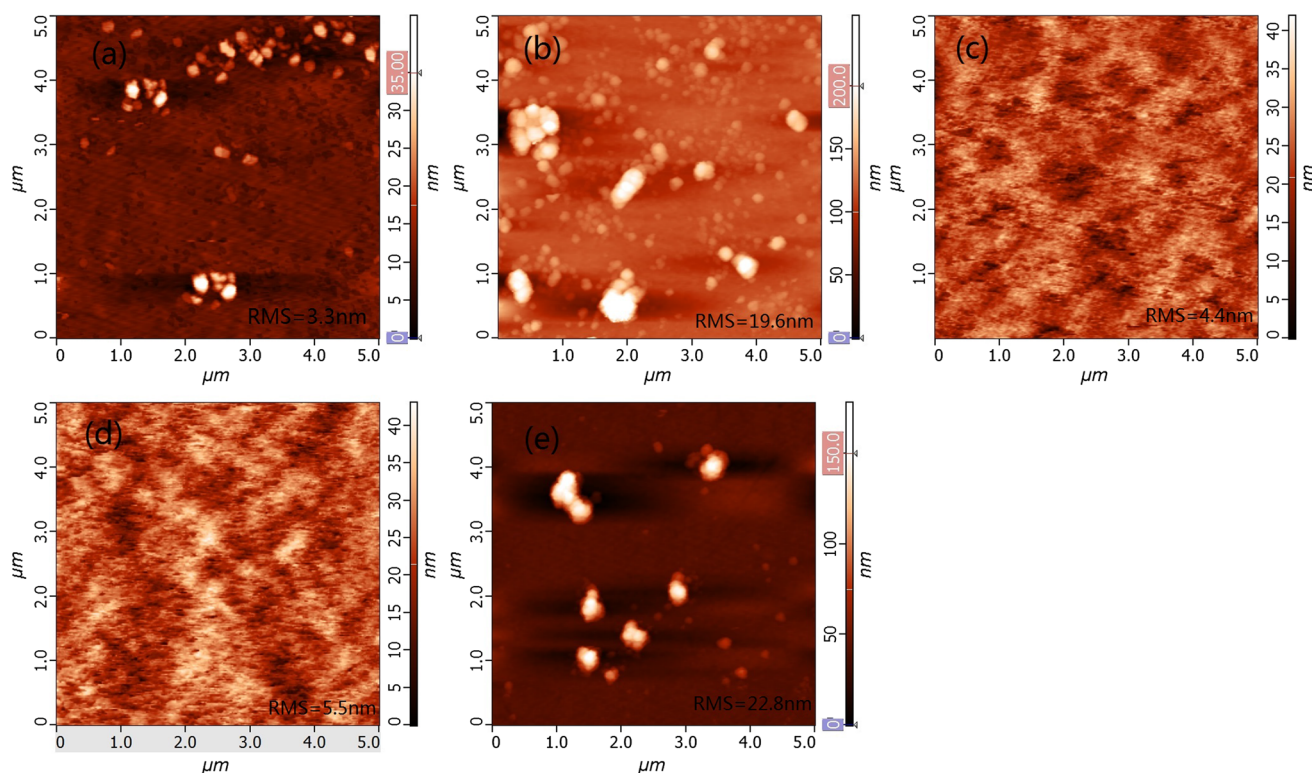


Fig. 4 AFM images of ZnO cathode buffer layer derived from ZnO NPs solutions with different methanol/*o*-dichlorobenzene ratios (v/v), **a** 0:100 %, **b** 20:80 %, **c** 40:60 %, **d** 50:50 %, **e** 100:0 %.

Comparative analysis images between aggregation variation of ZnO NPs and RMS roughness variation of ZnO nanofilm

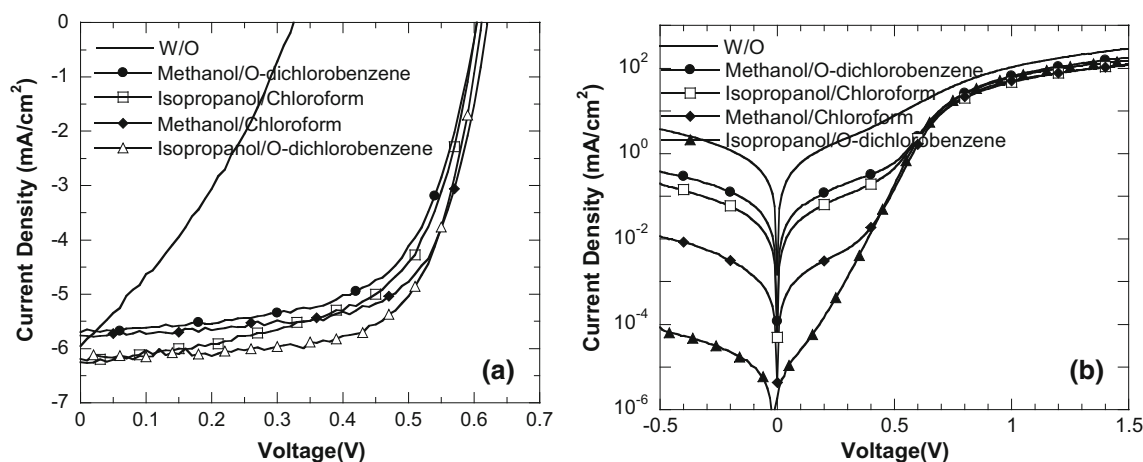


Fig. 5 Illuminated (a) and dark (b) J–V characteristics the inverted organic solar cells with buffer layers deposited from the ZnO NPs solution dispersed in different mixture of binary solvents

Table 4 The photovoltaic properties of the inverted organic solar cells with buffer layers deposited from the ZnO NPs solution dispersed in different mixture of binary solvents

Mixture	J_{sc} (mA/cm ²)	V_{oc} (V)	FF (%)	PCE (%)
None	5.96	0.33	0.32	0.62
Methanol/ <i>o</i> -dichlorobenzene (40:60)	5.70	0.60	0.63	2.16
Isopropanol/chloroform (50:50)	6.26	0.61	0.60	2.26
Methanol/chloroform (30:70)	5.76	0.62	0.67	2.40
Isopropanol/ <i>o</i> -dichlorobenzene (60:40)	6.20	0.61	0.67	2.55

Current density–voltage (J–V) characteristics of OSC including ZnO films deposited from solution dispersed in different composition under AM 1.5G irradiation with intensity of 100 mW/cm² and in dark are shown in Fig. 5. Table 4 summarizes the data of device parameters. We refer to that “x” the volume ratio of the solution mixtures of Table 2 are applied in this table. Here, the ratio of mixture of methanol/*o*-dichlorobenzene is 40:60, the ratio of isopropanol/chloroform is 50:50, the ratio of methanol/chloroform is 30:70, and the ratio of isopropanol/*o*-dichlorobenzene is 60:40. It can be observed that the device without ZnO cathode buffer layer exhibits the lowest PCE of 0.62 % and the device based on ZnO NPs dispersed in mixed solvent as the buffer layer exhibits the PCE of from 2.16 to 2.55 %. Chloroform which was classified as “good” solvent showed highly improved dispersion of ZnO NPs in mixing with methanol, a “bad” solvent [22]. However, in this study, *o*-dichlorobenzene was proved to be “better” solvents as non-polar for dispersion of ZnO NPs in mixing with methanol or isopropanol. With the dichlorobenzene mixing from methanol to isopropanol, the V_{oc} , J_{sc} , and FF of devices increase gradually, so the PCE increase from 0.62 to 2.16 and 2.55 %, respectively.

4 Conclusions

In summary, the performance of organic solar cells with ZnO NPs as buffer layer has been studied. ZnO NPs with a size of 3–5 nm were synthesized in solvothermal synthesis at low temperature, which exhibited a relatively wide photoluminescence peak. More importantly, based on Hansen solubility parameter theory, a mathematical method was found to calculate the dispersion of ZnO NPs in bi-solvent system, and the superior solvent ratios were obtained. AFM measurement shows that the morphology of ZnO buffer layers was highly improved by mixed solvents, and the aggregations and homogeneity of ZnO NPs are adjustable. The power conversion efficiency of the inverted device with the improved ZnO buffer layers was enhanced obviously. The results indicate that the bi-solvent system is a facile method for the interfacial modification in the fabrication of high-performance inverted organic solar cells.

Acknowledgments We gratefully acknowledge the financial support of National Natural Science Foundation of China (No. 11304045), and Guangdong provincial science and technology projects (Grant No. 2013B090700006).

References

1. F.C. Krebs, Fabrication and processing of polymer solar cells: a review of printing and coating techniques. *Sol. Energy Mater. Sol. Cells* **93**, 394–412 (2009)
2. H.L. Hsu, T.Y. Juang, C.P. Chen, C.M. Hsieh, C.C. Yang, C.L. Huang, R.J. Jeng, Enhanced efficiency of organic and perovskite photovoltaics from shape-dependent broadband plasmonic effects of silver nanoplates. *Sol. Energy Mater. Sol. Cells* **140**, 224–231 (2015)
3. K.D.G.I. Jayawardena, L.J. Rozanski, C.A. Mills, M.J. Beliatas, N.A. Nisamy, S.R.P. Silva, Inorganics-in-organics: recent developments and outlook for 4G polymer solar cells. *Nanoscale* **5**, 8411–8427 (2013)
4. H.Y. Park, I. Ryu, J. Kim, S. Jeong, S. Yim, S.Y. Jang, PbS quantum dot solar cells integrated with sol–gel-derived ZnO as an n-type charge-selective layer. *J. Phys. Chem. C* **118**, 17374–17382 (2014)
5. J. You, C.C. Chen, Z. Hong, K. Yoshimura, K. Ohya, R. Xu, S. Ye, J. Gao, G. Li, Y. Yang, 10.2 % power conversion efficiency polymer tandem solar cells consisting of two identical sub-cells. *Adv. Mater.* **25**, 3973–3978 (2013)
6. X.D. Dang, M. Dante, T.Q. Nguyen, Morphology and conductivity modification of poly(3,4-ethylenedioxythiophene):poly(styrene sulfonate) films induced by conductive atomic force microscopy measurements. *Appl. Phys. Lett.* **93**, 241911–241911-3 (2008)
7. K. Norrman, S.A. Gevorgyan, F.C. Krebs, Water-induced degradation of polymer solar cells studied by H₂¹⁸O labeling. *ACS Appl. Mater. Interfaces* **1**, 102–112 (2008)
8. K. Kawano, R. Pacios, D. Poplavskyy, J. Nelson, D.D.C. Bradley, J.R. Durrant, Degradation of organic solar cells due to air exposure. *Sol. Energy Mater. Sol. Cells* **90**, 3520–3530 (2006)
9. S. Trost, T. Becker, K. Zilberberg, A. Behrendt, A. Polywka, R. Heiderhoff, P. Görrn, T. Riedl, Plasmonically sensitized metal-oxide electron extraction layers for organic solar cells. *Sci. Rep.* **5**, 7765 (2015)
10. R. Lampande, G.W. Kim, J. Boizot, Y.J. Kim, R. Podeb, J.H. Kwon, A highly efficient transition metal oxide layer for hole extraction and transport in inverted polymer bulk heterojunction solar cells. *J. Mater. Chem. A* **1**, 6895 (2013)
11. Z.L. Yuan, J.S. Yu, N.N. Wang, Y.D. Jiang, Well-aligned ZnO nanorod arrays from diameter-controlled growth and their application in inverted polymer solar cell. *J. Mater. Sci. Mater. Electron.* **22**, 1730–1735 (2011)
12. Y. Lare, M. Banéto, L. Cattin, M. Morsli, K. Jondo, K. Napo, J.C. Bernède, Effect of a zinc oxide, at the cathode interface, on the efficiency of inverted organic photovoltaic cells based on the CuPc/C60 couple. *J. Mater. Sci. Mater. Electron.* **22**, 365–370 (2011)
13. Z. Lu, X.H. Chen, J.P. Zhou, Z.Y. Jiang, S.M. Huang, F.R. Zhu, X.Q. Piao, Z. Sun, Performance enhancement in inverted polymer solar cells incorporating ultrathin Au and LiF modified ZnO electron transporting interlayer. *Org. Electron.* **17**, 364–370 (2015)
14. J.J. Chang, Z. Lin, C.X. Zhu, C. Chi, J. Zhang, J. Wu, Solution-processed LiF-doped ZnO films for high performance low temperature field effect transistors and inverted solar cells. *ACS Appl. Mater. Interfaces* **5**, 6687–6693 (2013)
15. C. Pacholski, A. Kornowski, H. Weller, Self-assembly of ZnO: from nanodots to nanorods. *Angew. Chem. Int. Ed.* **41**, 1188–1191 (2002)
16. T. Chu, S. Tsang, J. Zhou, P.G. Verly, J. Lu, S. Beaupre, M. Leclerc, Y. Tao, High-efficiency inverted solar cells based on a low bandgap polymer with excellent air stability. *Sol. Energy Mater. Sol. Cells* **96**, 155–159 (2012)
17. Z. Ma, Z. Tang, E. Wang, M.R. Andersson, O. Inganäs, F. Zhang, Influences of surface roughness of ZnO electron transport layer on the photovoltaic performance of organic inverted solar cells. *J. Phys. Chem. C* **116**, 24462–24468 (2012)
18. W.J.E. Beek, M.M. Wienk, M. Kemerink, X. Yang, R.A.J. Janssen, Hybrid zinc oxide conjugated polymer bulk heterojunction solar cells. *J. Phys. Chem. B* **109**, 9505–9516 (2005)
19. W.J.E. Beek, M.M. Wienk, R.A.J. Janssen, Hybrid solar cells from regioregular polythiophene and ZnO nanoparticles. *Adv. Funct. Mater.* **16**, 1112–1116 (2006)
20. Y. Yao, J. Hou, Z. Xu, Y. Yang, Effects of solvent mixtures on the nanoscale phase separation in polymer solar cells. *Adv. Funct. Mater.* **18**, 1783–1789 (2008)
21. P.D. Li, T.G. Jiu, G. Tang, G.J. Wang, J. Li, X.F. Li, J.F. Fang, High-performance inverted solar cells based on blend films of ZnO nanoparticles and TiO₂ nanorods as cathode buffer layer. *ACS Appl. Mater. Interfaces* **6**, 18172–18179 (2014)
22. M.J. Tan, S. Zhong, J. Li, Z. Chen, W. Chen, Air-stable efficient inverted polymer solar cells using solution processed nanocrystalline ZnO interfacial layer. *ACS Appl. Mater. Interfaces* **5**, 4696–4701 (2013)
23. M. Dosmailov, L.N. Leonat, J. Patek, D. Roth, P. Bauer, M.C. Scharber, N.S. Sariciftci, J.D. Pedarnig, Transparent conductive ZnO layers on polymer substrates: thin film deposition and application in organic solar cells. *Thin Solid Films* **591**, 97–104 (2015)
24. B. Qi, J. Wang, Fill factor in organic solar cells. *Phys. Chem. Chem. Phys.* **15**, 8972–8982 (2013)
25. J. Luo, C.M. Liu, S.H. Yang, Y. Cao, Hybrid solar cells based on blends of poly(3-hexylthiophene) and surface dye-modified, ultrathin linear- and branched-TiO₂ nanorods. *Sol. Energy Mater. Sol. Cells* **94**, 501–508 (2010)
26. E.G. Barbagioanni, V. Strano, G. Franzo, I. Crupi, S. Mirabella, Photoluminescence transient study of surface defects in ZnO nanorods grown by chemical bath deposition. *Appl. Phys. Lett.* **106**, 093108 (2015)
27. S. Mehmood, M.A. Rehman, H. Ismail, B. Mirza, A.S. Bhatti, Significance of postgrowth processing of ZnO nanostructures on antibacterial activity against gram-positive and gram-negative bacteria. *Int. J. Nanomed.* **10**, 4521–4533 (2015)
28. T.V. Torchynska, B.E. Filali, Size dependent emission stimulation in ZnO nanosheets. *J. Lumin.* **149**, 54–60 (2014)
29. C.M. Hansen, *Hansen Solubility Parameters*, 2nd edn. (CRC Press, Boca Raton, 2007)
30. J. Ma, R.M. Larsen, Effect of surface modification on the hansen solubility parameters of single-walled carbon nanotubes. *Ind. Eng. Chem. Res.* **52**, 3514–3521 (2013)
31. H. Launay, C.M. Hansen, K. Almdal, Hansen solubility parameters for a carbon fiber/epoxy composite. *Carbon* **45**, 2859–2865 (2007)
32. K.C. Choi, E.J. Lee, Y.K. Baek, M.J. Kim, Modifying hydrogen bonding interaction in solvent and dispersion of ZnO nanoparticles: impact on the photovoltaic performance of inverted organic solar cells. *R. Soc. Chem.* **4**, 7160–7166 (2014)
33. Z. Ma, Z. Tang, E. Wang, M.R. Andersson, O. Inganäs, F. Zhang, Influences of surface roughness of ZnO electron transport layer on the photovoltaic performance of organic inverted solar cells. *J. Phys. Chem. C* **116**, 24462–24468 (2012)